OPTICA

Kramers–Kronig relation in attosecond transient absorption spectroscopy

Vyacheslav Leshchenko,[1,*] Stephen J. Hageman,[1] Coleman Cariker,[2] Gregory Smith,[1] Antoine Camper,[1,3] Bradford K. Talbert,[1] Pierre Agostini,[1] Luca Argenti,[2] and Louis F. DiMauro[1]

[1]Department of Physics, The Ohio State University, Columbus, Ohio 43210, USA
[2]Department of Physics and CREOL, University of Central Florida, Orlando, Florida 32816, USA
[3]Department of Physics, University of Oslo, Sem Sælandsvei 24, Oslo 0371, Norway
*Corresponding author: leshchenko.1@osu.edu

Received 8 September 2022; revised 19 November 2022; accepted 29 November 2022; published 24 January 2023

The Kramers–Kronig relation (KKR) has a wide range of applications in extreme ultraviolet (XUV) and x-ray spectroscopy. However, the validity of KKR for many of these applications has not been systematically studied, while it is known to require careful attention in nonlinear and pump–probe experiments in optical domain spectroscopy. Here, we study the validity of KKR in XUV attosecond transient absorption spectroscopy pump–probe measurements both experimentally and theoretically using argon Fano resonances as a case study. Experiments are enabled by a phase-resolved method dubbed Complex Attosecond Transient-absorption Spectroscopy (CATS). Although the estimations based on the rotating-wave approximation suggest that KKR violation could be expected in the studied case, our results validate KKR and provide a solid basis for its application in a broad range of attosecond spectroscopy experiments.

https://doi.org/10.1364/OPTICA.474960

1. INTRODUCTION

The Kramers–Kronig relation (KKR) is a powerful tool to study properties of materials in different fields of research and applications. Originally derived for linear electric susceptibility [1,2], it has been shown to be widely applicable to nonlinear optics [3]. However, in nonlinear and pump–probe experiments, KKR needs careful consideration since it is known to fail in some cases [3–5], typically due to the cross-phase modulation effect in the four-wave mixing nonlinear interaction. While KKR validity in nonlinear optics has been discussed for a few decades [3–5], it has not been addressed in attosecond physics in general or for pump–probe experiments involving extreme ultraviolet (XUV) pulses in particular. Nonetheless, KKR is often used in XUV and x-ray absorption and reflection spectroscopy [6,7] including pump–probe experiments [8] to reconstruct the real part of the electric susceptibility (refractive index) from its imaginary part (absorption), which is experimentally much more accessible in the XUV spectral range. In this paper, we systematically study the applicability of KKR to pump–probe attosecond transient absorption spectroscopy (ATAS) experiments both theoretically and experimentally.

In a standard pump–probe ATAS experiment [9–12] the validity of KKR can be fundamentally questioned based on the details of experiments, as the change of the spectral transmittance/absorbance of the XUV attosecond pulse or pulse train is measured as a function of the delay to the dressing optical pulse. In the case of ultrashort pulses, the transmittance of the XUV pulse can be modified by an optical pulse interacting with the medium outside of the temporal overlap with the XUV pulse. This can be interpreted as a violation of causality, the foundation of KKR, since the XUV absorbance is modified by an optical pulse at a later time. However, it is important to note that there is no global causality violation after taking into consideration the lifetime of excited states. Thus, the validity of the standard KKR in this type of experiment is a nontrivial question that requires careful considerations. Moreover, it has been experimentally demonstrated that KKR fails under some conditions in pump–probe TAS experiments in the optical domain [4,5].

In a three-level system composed of a ground state radiatively coupled to a bright state by XUV, and a dark state coupled to the bright state by IR (see Supplement 1 for details), in the rotating-wave approximation (RWA), the pump-induced part of susceptibility (χ) is diagonal: $\tilde{\mu}(\omega) \propto \tilde{\chi}(\omega)\tilde{E}_{\mathrm{XUV}}(\omega)$. $\tilde{E}_{\mathrm{XUV}}(\omega)$ and $\tilde{\mu}(\omega)$ are the Fourier transforms of the electric field $E_{\mathrm{XUV}}(t)$ of the XUV pulse and of the expectation value of the dipole moment $\mu(t) = \langle\Psi(t)|\hat{\mu}_z|\Psi(t)\rangle$, respectively. Therefore, the electric susceptibility is analytical in the upper complex plane, and the KKR is satisfied [3]. Thus, when the effect of the dressing laser is just to couple one bright and one dark state, the KKR is expected to be satisfied.

However, as can be identified in the level diagram of argon in Fig. 1(c), the situation is more complicated when it is dressed at 1350 nm, as in our experiments, since multiple bright and dark

states are resonantly coupled. As can be shown in a relatively simple analysis of a four-level system based on RWA, presented in Supplement 1 (with the following levels: ground; bright_1; dark; bright_2; the last three are spaced with the optical pulse photon energy), the susceptibility is non-diagonal, i.e., the system does not respond only at the same frequency as the excitation, but also at frequencies given by the difference in energy between excited states:

$$\tilde{\chi}(\omega) = \sum_{jk} \chi_{jk}(\omega - \omega_{jk}) \frac{\tilde{E}_{\mathrm{XUV}}(\omega - \omega_{jk})}{\tilde{E}_{\mathrm{XUV}}(\omega)}, \quad (1)$$

where ω_{jk} is the frequency (energy) spacing between states. All the $\chi_{jk}(\omega)$ are analytical in the upper complex semi-plane. However, $\tilde{\chi}(\omega)$ depends on the ratio $\tilde{E}_{\mathrm{XUV}}(\omega - \omega_{jk})/\tilde{E}_{\mathrm{XUV}}(\omega)$, which, in general, cannot be assumed to be analytical in the upper semi-plane. Therefore, KKR is not expected to be satisfied for such a system, which is a simplified model of the sample in the experiment.

In this work, we study the validity of KKR in XUV ATAS pump–probe measurements both experimentally and theoretically using argon Fano resonances as a case study. Experiments are enabled by a new phase-resolved method dubbed complex attosecond transient-absorption spectroscopy (CATS). Although the estimations based on the RWA suggest that KKR violation could be expected in the studied case, our results validate KKR and provide a solid basis for its application in a broad range of attosecond spectroscopy experiments.

2. EXPERIMENTAL SETUP

KKR cannot be tested in the standard ATAS setup, as it provides direct experimental access only to absorbance ($\tilde{\beta}(\omega) \propto \Im m[\tilde{\mu}(\omega)/\tilde{E}(\omega)]$), which is proportional to the imaginary part of the dipole moment and the corresponding electric susceptibility. To access the real part of the electric susceptibility, it is necessary to measure the real part of the refractive index.

We have developed a modified ATAS setup (Fig. 1) that provides access to both real and imaginary parts of the electric susceptibility by measuring the complex refractive index, which directly tests KKR. We dubbed the technique as Complex Attosecond Transient-absorption Spectroscopy (CATS), which can simultaneously measure both parts of the complex electric susceptibility of a sample. The most straightforward and reliable way to measure the phase of an electromagnetic wave is an interferometer. The standard Mach–Zehnder scheme, which naively might be considered as an option, is not applicable in the XUV spectral range due to the absence of XUV beam splitters. Thus, an alternative scheme without transmissive optics is required. The alternative to the Mach–Zehnder interferometer is the Young's interferometer [Fig. 1(b)], which can be realized in a full-reflection approach [Fig. 1(a)]. The key step towards its realization is the generation of two phase-locked spatially separated sources, which in our experiment is realized with a two-source high harmonic generation (HHG) [13,14] based on a two-focus driving beam generated with a binary $0-\pi$ phase grating [13]. It is a more reliable modification of the birefringent scheme introduced a few decades ago [14].

The experimental setup is schematically shown in Fig. 1. 1350 nm (0.91 eV) pulses with 50 fs duration and 3 mJ energy at 1 kHz repetition rate are generated in an optical parametric amplifier (OPA) HE-TOPAS Prime (Light-Conversion) pumped with a Ti:sapphire laser system (Spitfire Ace, Spectra-Physics). The OPA output is split into two parts: 92% of power is used for HHG, and 8% is used for the dressing beam. The two foci are generated by a $0-\pi$ phase grating [13] with a 2.5 mm period, which results in focus separation of 430 μm for a 40 mm focal length lens. HHG is generated in an argon gas jet created by a pulsed valve with a conical nozzle (Even-Lavie [15]). The residual near-IR (NIR) radiation is filtered with a 200 nm thick aluminum filter. The generated XUV radiation is refocused on a sample with an ellipsoidal mirror with

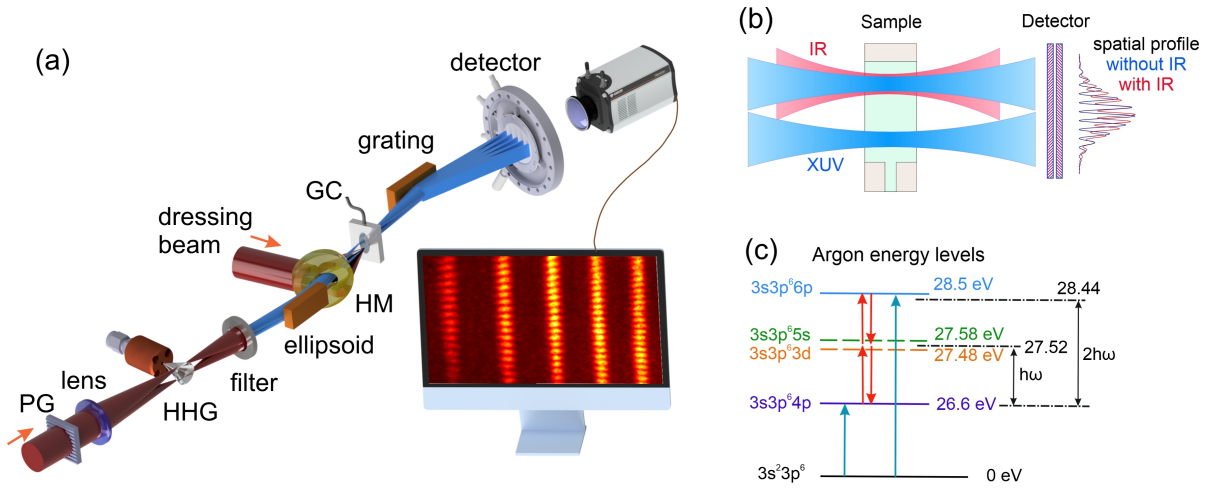

Fig. 1. (a) Scheme of the experimental setup of complex attosecond transient-absorption spectroscopy (CATS). PG, phase grating; HM, hole mirror; GC, gas cell; HHG, high harmonic generation. The measurement of both imaginary and real parts of the electric susceptibility is realized through the interference of two phase-locked XUV HHG beams (an example of measured spectrally resolved interference is shown in the bottom-right inset). The dressing-(IR) beam-induced change in the real part of the susceptibility is measured from the shift of the interference fringes; the dressing-induced modification of the imaginary part of susceptibility is determined from the visibility change. Two HHG beams are generated with a two-focus IR beam, which is accomplished by a $0-\pi$ phase grating [13]. The dressing beam is overlapped with one of the XUV beams using a hole mirror. The XUV spectrum after the sample is measured with a flat-field spectrometer. (b) Principle of XUV Young's interferometer to measure complex sample electric susceptibility. (c) Argon energy level diagram and dressing-induced coupling for the experimental wavelength of 1350 nm.

3× demagnification, so the separation between the XUV foci in the sample plane is about 140 μm. Both XUV foci have diameters of 12 μm as measured with a knife-edge method. The XUV spectrum after the sample is measured with a spectrometer based on a curved variable line space grating from Hitachi (1200 l/mm) and a microchannel plate chevron with a phosphor screen. The phosphor screen is imaged onto an Andor Neo 5.5 CMOS camera.

The dressing beam is focused with a lens located outside of the vacuum chamber, coupled in the chamber through a CaF_2 window and overlapped with one of the XUV beams using a hole mirror (Fig. 1). The power and polarization of the dressing beam are controlled with a combination of two polarizers and a half-wave plate. The delay between the HHG pulses and the dressing beam is controlled with a motorized pair of wedges in the dressing arm. The dressing beam has a full width half maximum (FWHM) diameter of 34 μm, which is significantly smaller than the separation of the XUV sources and enables reliable dressing of only one XUV beam. The dressing intensity was characterized by measuring spatial and temporal pulse profiles. Pulse duration was characterized with a home-built second-harmonic generation frequency-resolved optical gating (SHG-FROG) setup. The spatial distribution at the position of the gas cell was characterized by imaging the beam onto a camera (Goldeye SWIR InGaAs) with an infinity corrected microscopic objective with 20× magnification (20X EO M Plan Apo).

The sample is a 2 mm long gas cell with 750 μm × 250 μm aperture (height × width), which is backed with 60 Torr of argon. The aperture of the gas cell allows both XUV sources to pass through the gas medium without being clipped.

3. RESULTS AND DISCUSSION

In our experiments, one of the harmonic orders generated by the 1350 nm pulses is centered at the $3s^{-1}4p$ Ar Fano resonance (26.6 eV) and excites it. At the same time, the 1350 nm dressing pulse provides resonant coupling between $3s^{-1}4p$ bright state and $3s^{-1}3d$, $3s^{-1}5s$ dark states, and $3s^{-1}6p$ bright state [Fig. 1(c)]. It is a nontrivial case with simultaneous coupling of multiple bright and dark states [12], which is a very interesting scenario for the test of KKR.

The measured dependence of XUV absorbance $\Delta\mathrm{OD} = \log_{10}(I_{\mathrm{XUV}}/I_{\mathrm{XUV+IR}})$ (change of optical density) and phase $\Delta\Phi = \Phi_{\mathrm{XUV}} - \Phi_{\mathrm{XUV+IR}}$ (change of phase corresponding to the change of the refractive index) on the dressing pulse intensity is shown in Fig. 2. The data are taken at the temporal overlap between XUV and dressing pulses.

For a better understanding of the underlying physics, the experimental results are compared to *ab initio* theoretical calculations, which are also presented in Fig. 2 (see Supplement 1 for more details). The theoretical calculations are based on the NewStock suite of codes [16,17]. In the simulations, localized orbitals are computed using the multi-configurational Hartree–Fock algorithm, with the assistance of the ATSP2K atomic structure package, optimized on the $3s^{-1}$ and $3p^{-1}$ parent ion configurations. The basis for neutral argon is composed of configurations of localized orbitals augmented by close-coupling channels, where parent ion state configurations are coupled to a spherical harmonic and radial B-splines that represent the residual electron. The evolution of the system $\Psi(t)$ under the influence of external fields is computed by numerically solving the time-dependent

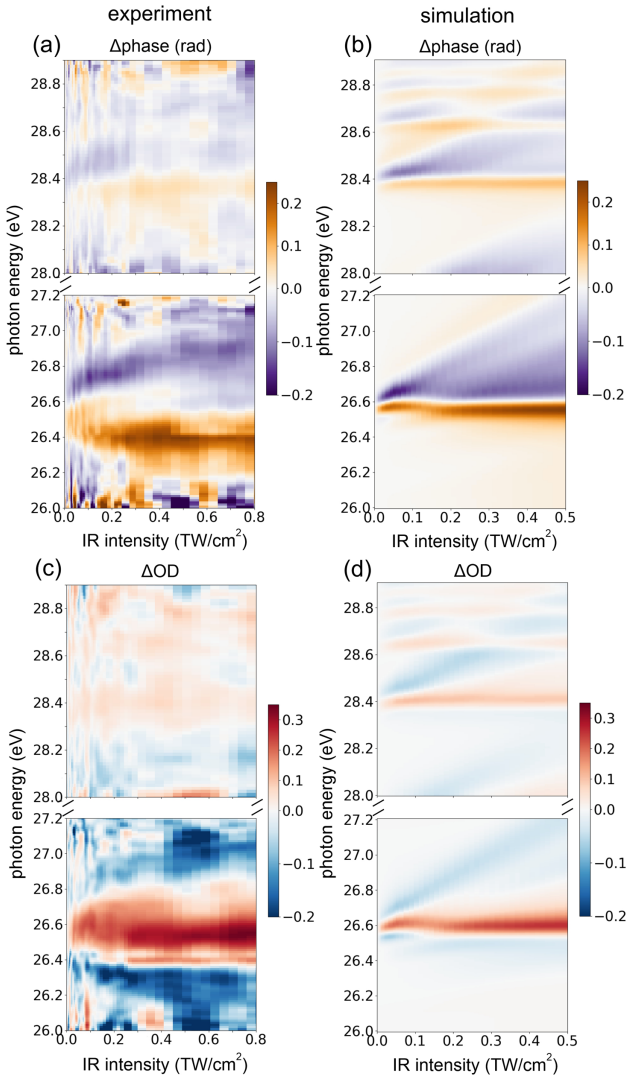

Fig. 2. Experimentally measured change in XUV phase (a) and absorbance (c) and the corresponding simulation results for phase (b) and absorbance (d). Results are obtained at 1350 nm optical wavelength with parallel linear polarizations of both pump and probe. The break in the photon energy (y) axis between 27.2 and 28 eV is caused by the spectral region between the HHG harmonics with no signal above the noise level [see the HHG spectrum in Fig. 3(c)]. The simulation intensity range is chosen to best fit the features in the measurement, which results in a slightly different intensity scale.

Schrödinger equation (TDSE) using a split-exponential propagator, within the dipole approximation and in the velocity gauge. For optically thin samples, the absorption spectrum is then calculated as $\sigma(\omega) = \frac{4\pi}{\omega}\Im m[\tilde{P}(\omega)/\tilde{A}(\omega)]$, where $P(\omega)$ and $A(\omega)$ are the Fourier transform of the expectation value of the canonical momentum $P(t) = \langle\Psi(t)|\hat{P}_z|\Psi(t)\rangle$ and of the vector potential $A_z(t)$ of the XUV pulse, respectively. The simulations are performed for a fixed optical peak intensity, which corresponds to one point in the focal volume in the experiment. To account for the focal volume intensity distribution in experiments, an averaging over the focal volume distribution was applied to theoretical data in the presented results (Fig. 2). The experimental focal intensity distribution was measured by recording a number of images of the dressing beam at a set of distances from the focus.

The results in Fig. 2 show that there is a good agreement between experiments and simulations in both phase and optical density, as most of the main features at Fano resonances are reproduced ($3s^{-1}4p$ resonance at around 26.6 eV; $3s^{-1}6p$ at around 28.4 eV; $3s^{-1}7p$ at around 28.65 eV), although there is a small disagreement in absolute dressing intensity, e.g., the increases of the amplitude, spectral broadening, and shift of these features are well reproduced. The mentioned minor discrepancy between experiments and simulations in the absolute intensity values is attributed to the uncertainties in the measurement of the experimental focal volume intensity distribution and in applying it to simulations with discrete intensity steps. Details on the nature of the shape and fine structures in the argon Fano resonances can be found elsewhere [18].

KKR validity is tested by taking slices at fixed intensities and computing the real part of the electric susceptibility from the imaginary one. The result at 0.25 TW/cm^2 is shown in Fig. 3 as an example. Both experiment and simulation show perfect agreement between the measured phase and the signal reconstructed from absorbance using KKR, which is observed in the full intensity range available in the experiment. It is also the case for all nonzero delays between XUV and optical pulses, as can be seen in the delay scan presented in Supplement 1. Note that the presented spectral range is large enough for the reliable application of KKR to the resonances, namely, it was tested that the extension or slight reduction of the ΔOD range used in the KKR reconstruction causes no significant change of the reconstructed phase.

The obtained confirmation of the fact that KKR is satisfied even in a quite complex system is an important and nontrivial result, which is discussed in the following.

If we analyze Eq. (1) describing the susceptibility in a four-level system in RWA, the electric susceptibility becomes an average of analytic functions (χ_{jk}) for a short enough XUV pulse $E_{\mathrm{XUV}}(t)$, as the XUV spectral intensity $\tilde{E}_{\mathrm{XUV}}(\omega)$ is essentially constant across the resonance (Fano resonance here). In this case, $\tilde{\chi}$ is analytical, and KKR is satisfied. This condition can be formulated as

$$\mathrm{Width}[\tilde{E}_{\mathrm{XUV}}(\omega)] \gg \mathrm{Width}[\tilde{\chi}_{\mathrm{resonance}}(\omega)]. \tag{2}$$

The condition in Eq. (2) is always satisfied for isolated attosecond pulses (IAPs) for all processes on femtosecond and longer time scales. This conclusion validates applicability of KKR in linear ATAS (when nonlinear XUV effects can be neglected) with IAP, which presently covers a significant portion of all ATAS studies; thus, it has a very high general importance for the ATAS field. In addition, it is an alternative explanation of the successful time-dependent dipole reconstruction results in Ref. [8].

However, here, we have an attosecond pulse train instead of IAP due to a multi-cycle duration of the optical pulse driving HHG. Nonetheless, the width of XUV harmonics is about three to four times larger than the argon Fano resonances' widths. In addition, harmonics in the range of the resonances are from the HHG plateau with almost identical shape and width. Thus, $\tilde{E}_{29}(\omega - \omega_{6p-4p})/\tilde{E}_{31}(\omega) \approx$ constant, where harmonics 29 and 31 overlap with the 4p and 6p resonances, respectively. Therefore, the electric susceptibility can be expressed as an average of analytic functions $\tilde{\chi}(\omega) \approx \sum_{jk} \chi_{jk}(\omega - \omega_{jk})$ in the considered case as well, and KKR is satisfied.

It is worth mentioning that the developed experimental technique will be highly valuable for XUV–XUV and x-ray–x-ray pump–probe studies where KKR is expected to fail in some cases,

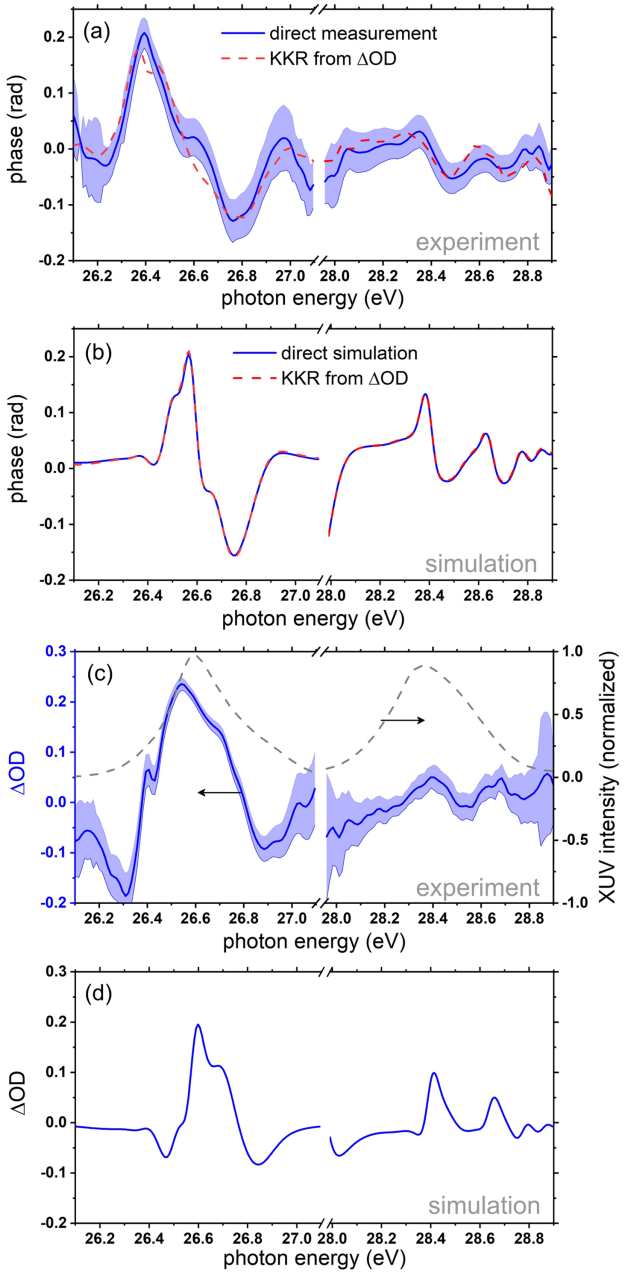

Fig. 3. Comparison between direct measurement of the real dipole response and the KK reconstruction for experiment (a) and simulation (b). (c), (d) Corresponding imaginary parts used in KK reconstruction. The light blue area around the main curve represents the uncertainty (standard deviation) of the experimental data. The dashed gray line in (c) is the HHG intensity spectral distribution. Results are obtained at 1350 nm optical wavelength with parallel linear polarization of both pump and probe.

e.g., when four-wave-mixing is involved, as it was demonstrated in the optical domain [3–5]. In addition, the presented approach of the direct measurement of complex susceptibility will be valuable for experiments with more complicated systems where the KKR applicability is limited by, e.g., the experimentally accessible spectral range, whereas the phase is measured directly in CATS, and the spectral range is not crucial. Another promising application of the CATS technique is the single-shot reconstruction of a full (complex) temporal dipole [8], which can be realized in laser systems with low repetition rates, e.g., sources driven by ~PW laser

systems, or with an unstable pulse spectrum and/or arrival time, e.g., free electron lasers. One more useful advantage of CATS compared to the standard ATAS is the possibility to improve the signal to noise ratio when it is limited by the intensity instability of the XUV source, as CATS is a two-beam self-normalizing technique where the identical intensity fluctuations in both beams do not affect the measurement (when XUV intensity is below the onset of nonlinear effects).

4. SUMMARY

In conclusion, the validity of the KKR in XUV ATAS pump–probe experiments is studied both experimentally and theoretically. The experimental study is enabled by the CATS technique introduced here. Although a gas-phase absorption spectroscopy is realized here, the technique can be easily extended to any sample type in both absorption and reflection configurations. The results presented in the paper validate KKR for a nontrivial case, with multiple bright and dark states being coupled. It provides a solid basis for KKR application in a broad range of attosecond spectroscopy experiments, e.g., XUV transient absorption and reflection studies. In addition, we believe that the developed and presented CATS experimental technique could enable and/or advance a broad range of applications in XUV and x-ray spectroscopy.

Funding. Air Force Office of Scientific Research (FA-9550-15-1-0037); U.S. Department of Energy (DE-GF02-04ER15614); National Science Foundation (N 1607588, N 1912507).

Acknowledgment. L.A. and C.C. acknowledge computer time at the University of Central Florida Advanced Research Computing Center. The authors acknowledge Enam Chowdhury for lending a SWIR camera for the NIR beam profile characterization. The experiments were conducted at The Ohio State University and supported by the U.S. AFOSR. A.C. was supported by the Department of Energy. L.A. and C.C. acknowledge support from the NSF Theoretical AMO.

Disclosures. The authors declare no conflicts of interest.

Data availability. Data underlying the results presented in this paper are not publicly available at this time but may be obtained from the authors upon reasonable request.

Supplemental document. See Supplement 1 for supporting content.

REFERENCES

1. H. A. Kramers, "La diffusion de la lumiere par les atomes," Atti Cong. Intern. Fisica Como **2**, 545–557 (1927) [Transactions of Volta Centenary Congress].
2. R. de L. Kronig, "On the theory of dispersion of x-rays," J. Opt. Soc. Am. **12**, 547–557 (1926).
3. D. C. Hutchings, M. Sheik-Bahae, D. J. Hagan, and E. W. Van Stryland, "Kramers-Krönig relations in nonlinear optics," Opt. Quantum Electron. **24**, 1–30 (1992).
4. E. Tokunaga, A. Terasaki, and T. Kobayashi, "Femtosecond time-resolved dispersion relations studied with a frequency-domain interferometer," Phys. Rev. A **47**, R4581–R4584 (1993).
5. H. Kano and T. Kobayashi, "Simultaneous measurement of real and imaginary parts of nonlinear susceptibility for the verification of the Kramers–Kronig relations in femtosecond spectroscopy," Opt. Commun. **178**, 133–139 (2000).
6. H. R. Philipp and H. Ehrenreich, "Optical properties of semiconductors," Phys. Rev. **129**, 1550–1560 (1963).
7. R. Géneaux, C. J. Kaplan, L. Yue, A. D. Ross, J. E. Bækhøj, P. M. Kraus, H.-T. Chang, A. Guggenmos, M.-Y. Huang, M. Zürch, K. J. Schafer, D. M. Neumark, M. B. Gaarde, and S. R. Leone, "Attosecond time-domain measurement of core-level-exciton decay in magnesium oxide," Phys. Rev. Lett. **124**, 207401 (2020).
8. V. Stooß, S. M. Cavaletto, S. Donsa, A. Blättermann, P. Birk, C. H. Keitel, I. Březinová, J. Burgdörfer, C. Ott, and T. Pfeifer, "Real-time reconstruction of the strong-field-driven dipole response," Phys. Rev. Lett. **121**, 173005 (2018).
9. S. R. Leone, C. W. McCurdy, J. Burgdörfer, *et al.*, "What will it take to observe processes in real time?" Nat. Photonics **8**, 162–166 (2014).
10. C. Ott, A. Kaldun, L. Argenti, P. Raith, K. Meyer, M. Laux, Y. Zhang, A. Blättermann, S. Hagstotz, T. Ding, R. Heck, J. Madroñero, F. Martín, and T. Pfeifer, "Reconstruction and control of a time-dependent two-electron wave packet," Nature **516**, 374–378 (2014).
11. M. Wu, S. Chen, S. Camp, K. J. Schafer, and M. B. Gaarde, "Theory of strong-field attosecond transient absorption," J. Phys. B **49**, 062003 (2016).
12. N. Harkema, C. Cariker, E. Lindroth, L. Argenti, and A. Sandhu, "Autoionizing polaritons in attosecond atomic ionization," Phys. Rev. Lett. **127**, 023202 (2021).
13. A. Camper, H. Park, S. J. Hageman, G. Smith, T. Auguste, P. Agostini, and L. F. DiMauro, "High relative-phase precision beam duplicator for mid-infrared femtosecond pulses," Opt. Lett. **44**, 5465–5468 (2019).
14. R. Zerne, C. Altucci, M. Bellini, M. B. Gaarde, T. W. Hänsch, A. L'Huillier, C. Lyngå, and C.-G. Wahlström, "Phase-locked high-order harmonic sources," Phys. Rev. Lett. **79**, 1006–1009 (1997).
15. U. Even, "Pulsed supersonic beams from high pressure source: simulation results and experimental measurements," Adv. Chem. **2014**, 636042 (2014).
16. T. Carette, J. M. Dahlström, L. Argenti, and E. Lindroth, "Multiconfigurational Hartree-Fock close-coupling ansatz: application to the argon photoionization cross section and delays," Phys. Rev. A **87**, 023420 (2013).
17. A. Chew, N. Douguet, C. Cariker, J. Li, E. Lindroth, X. Ren, Y. Yin, L. Argenti, W. T. Hill, and Z. Chang, "Attosecond transient absorption spectrum of argon at the $L_{2,3}$ edge," Phys. Rev. A **97**, 031407 (2018).
18. S. Yanez-Pagans, C. Cariker, M. Shaikh, L. Argenti, and A. Sandhu, "Multipolariton control in attosecond transient absorption of autoionizing states," Phys. Rev. A **105**, 063107 (2022).